New orthorhombic modification of equiatomic CePdAl

2006 J. Phys.: Condens. Matter 18 9593

(http://iopscience.iop.org/0953-8984/18/42/006)

INSTITUTE OF PHYSICS PUBLISHING JOURNAL OF PHYSICS: CONDENSED MATTER

J. Phys.: Condens. Matter **18** (2006) 9593–9602 doi:10.1088/0953-8984/18/42/006

New orthorhombic modification of equiatomic CePdAl

A Gribanov[1], A Tursina[1], E Murashova[1], Y Seropegin[1], E Bauer[2,4], H Kaldarar[2], R Lackner[2], H Michor[2], E Royanian[2], M Reissner[2] and P Rogl[3]

[1] Department of Chemistry, Moscow State University, 119992 Moscow, Russia
[2] Institute of Solid State Physics, Vienna University of Technology, A-1040 Wien, Austria
[3] Institute of Physical Chemistry, University Vienna, A-1090 Wien, Austria

E-mail: bauer@ifp.tuwien.ac.at

Received 20 June 2006, in final form 15 September 2006
Published 5 October 2006
Online at stacks.iop.org/JPhysCM/18/9593

Abstract

The crystal structure of a new low-temperature modification of CePdAl was determined from single-crystal x-ray data: CePdAl-type; space group *Pmmn* (No. 59), $Z = 14$, oP42, $a = 0.426\,07$ nm, $b = 2.887\,58$ nm, $c = 0.721\,90$ nm; $R_F = 0.048$. Physical properties of orthorhombic CePdAl are governed by a mutual balance of the RKKY interaction, the Kondo effect and crystalline electric field splitting, resulting in antiferromagnetic ordering below ≈2.5 K. Electronic transport is reminiscent of a textbook-like Kondo lattice, which comes along with a significant negative magnetoresistance of more than 50% at low temperatures. Although geometrical frustration is absent when compared to the hexagonal modification of CePdAl, the ordering temperature T_N is even smaller. A possible cause is enhanced Kondo interactions.

(Some figures in this article are in colour only in the electronic version)

1. Introduction

Intermetallic rare-earth compounds have been the subject of thorough studies for many years, with promising applications. In addition, they are also a rich playground for studies of those principal interactions responsible for macroscopic phenomena such as superconductivity, long-range magnetic order, heavy fermion behaviour, metal-to-insulator transition, and many more.

The family of the equiatomic rare-earth compounds REPdAl has been reported to form in the orthorhombic TiNiSi-type of structure for RE = Sm, Gd. . . Tm, Y, isostructural to REPtAl (RE = Sm, Gd,. . . Tm, Lu, Y) [1], which is an ordered version of the Co_2Si type. This initial study was extended by Hulliger [2], who demonstrated that a high-temperature modification of REPdAl exists, crystallizing in the hexagonal ZrNiAl type of structure (RE = Sm, Gd. . .

[4] Author to whom any correspondence should be addressed.

Tm, Y). Antiferromagnetic order was found for RE = Tb, Dy, while HoPdAl exhibits a ferromagnetic instability. Hulliger could also show that a specific heat treatment allows us to stabilize this hexagonal structure for the Pr-, and Nd-based compounds as well. LaPdAl, however, is only available in a different modification (orthorhombic LaNiAl type).

In the present investigation we evidence that a novel type of structure exists for a low-temperature modification of CePdAl. Thus, the aim of this study is a detailed report on the structural properties together with a thorough investigation of bulk properties of this novel compound.

Hexagonal CePdAl was recently studied in detail and characterized as an antiferromagnetically ordered Kondo compound ($T_N = 2.7$ K) exhibiting a significant Sommerfeld value of $\gamma \approx 270$ mJ mol^{-1} K^{-2} [3, 4]. The spin structure is incommensurate along the *c*-axis with a propagation vector $\vec{k} = (1/2, 0, \approx 0.35)$. Remarkably, a third of all spins remain paramagnetic below the transition temperature [4]. Nuclear magentic resonance (NMR) measurements carried out by Nishiyama *et al* [5] evidenced a second phase transition at $T_{N2} \approx 1$ K. Long-range magnetic order, however, vanishes above 10 kbar, enabling non-Fermi liquid behaviour [6]. The triangular co-ordinated Ce ions in the hexagonal modification were said to give rise to geometrical frustration. As a consequence, the transition temperature appears to be reduced with respect to the actual exchange energy. Furthermore, the Kondo effect will additionally abate the ordering temperature.

2. Experimental details

For single-crystal determination and the measurement of physical properties, an alloy of about 1 g with a nominal composition of CePdAl was synthesized by arc melting ingots of the pure elements under Ar on a water-cooled copper hearth. The regulus was heat treated in an evacuated quartz tube at 900 °C for 10 days prior to quenching the silica capsule in water. X-ray intensity data were collected on a four-circle CAD-4 Enraf-Nonius diffractometer employing graphite monochromated Mo Kα radiation ($\lambda = 0.071\,073$ nm) from a suitable single crystal selected from the inner part of the alloy specimen. Absorption correction was made via one psi-scan. The crystal structure of *o*-CePdAl was solved by direct methods (SHELXS97 [7]) and refined by full-matrix least-squares procedures in the anisotropic approximation (SHELXL97 [7]). X-ray powder diffraction experiments were performed with a HUBER-670 image plate camera (Cu Kα_1-radiation, Ge standard). For Rietveld refinement we applied FULLPROF [8] and WinPLOTR [9] programs. Physical bulk properties were determined using a number of standard techniques, as described, for example, in [10].

3. Results and discussion

Conditions for x-ray single-crystal data collection are listed in table 1. A first structure model was obtained from direct methods and satisfactorily refined to low residual values, revealing a novel orthorhombic low-temperature modification of CePdAl (*o*-CePdAl). The refined structure after standardization with the program STRUCTURE TIDY [11] is presented in table 1. A Rietveld refinement of the corresponding x-ray powder data arrived at a residual value of $R_F = 0.050$, confirming the atom arrangement (see figure 1).

All atoms in the structure are situated in layers at $x = 1/4$ or $x = 3/4$. Coordination polyhedra around cerium atoms, Ce1, Ce2, Ce3 and Ce4, are pentagonal prisms with five additional atoms capping the lateral faces of the prisms (coordination number CN = 15). All Pd1–Pd4 atoms are located inside triangular prisms with three additional atoms around the waist of the prism (CN = 9). Aluminium atoms are surrounded by 12 atoms forming

Table 1. Crystal structure and relevant parameters of orthorhombic CePdAl.

Stucture type	Unique, orthorhombic CePdAl
Space group	$Pmmn$, No. 59, origin at $\bar{1}$
Lattice parameters (nm)	$a = 0.426\,07(5)$
	$b = 2.887\,58(10)$
	$c = 0.721\,90(8)$
Cell volume (nm^3)	0.888 16(15)
Number of formula units per cell, Z	14
Density, D_x (g/cm^3)	7.16
Crystal size (mm)	$0.03 \times 0.03 \times 0.03$
Radiation used in x-ray experiment (nm)	Mo Kα, 0.071 073
Absorption coefficient, μ (mm^{-1})	24.73
Data collection at room temperature	Enraf-Nonius CAD-4 autodiffractometer
	$-5 \leqslant h \leqslant 6$; $-33 \leqslant k \leqslant 44$; $-11 \leqslant l \leqslant 8$
Type of scanning; Θ range (deg)	$\omega/2\theta$; 1–33
Measured reflections; independent reflections	6639; 1863
Number of reflections with $I > 2\sigma(I)$	1616
R_{int}	0.063
Number of variables	68
$R[F^2 > 2\sigma(F^2)]$	0.048
$wR(F^2)$	0.134
GOF	1.047
Extinction	0.0052(4)
Atom positions[a]	
Ce1 in 4e	(1/4, 0.033 14(2), 0.644 50(9))
occ. = 1.00(4)	$U_{11} = 0.0093(3)$; $U_{22} = 0.0058(3)$; $U_{33} = 0.0038(3)$; $U_{23} = 0.0008(2)$[b]
Ce2 in 4e	(1/4, 0.126 83(2), 0.006 38(9))
occ. = 1.00(4)	$U_{11} = 0.0010(3)$; $U_{22} = 0.0048(3)$; $U_{33} = 0.0025(3)$; $U_{23} = 0.0003(2)$[b]
Ce3 in 4e	(1/4, 0.158 79(2), 0.512 14(9))
occ. = 1.00(4)	$U_{11} = 0.0092(3)$; $U_{22} = 0.0047(3)$; $U_{33} = 0.0017(3)$; $U_{23} = -0.000\,68(19)$[b]
Ce4 in 2a	(1/4, 1/4, 0.141 96(13))
occ. = 1.00(4)	$U_{11} = 0.0098(4)$; $U_{22} = 0.0051(4)$; $U_{33} = 0.0024(4)$[c]
Pd1 in 4e	(1/4, 0.040 67(3), 0.207 47(12))
occ. = 1.00(4)	$U_{11} = 0.0069(3)$; $U_{22} = 0.0057(4)$; $U_{33} = 0.0032(4)$; $U_{23} = 0.0003(3)$[b]
Pd2 in 4e	(1/4, 0.602 82(3), 0.276 03(13))
occ. = 1.00(4)	$U_{11} = 0.0088(4)$; $U_{22} = 0.0100(4)$; $U_{33} = 0.0056(4)$; $U_{23} = -0.0007(3)$[b]
Pd3 in 4e	(1/4, 0.677 58(3), 0.778 67(14))
occ. = 1.00(6)	$U_{11} = 0.0096(4)$; $U_{22} = 0.0091(4)$; $U_{33} = 0.0069(4)$; $U_{23} = 0.0001(3)$[b]
Pd4 in 2a	(1/4, 1/4, 0.721 63(18))
occ. = 1.00(4)	$U_{11} = 0.0069(5)$; $U_{22} = 0.0062(5)$; $U_{33} = 0.0040(5)$[c]
Al1 in 4e	(1/4, 0.534 88(13), 0.0101(5))
occ. = 1.00(7)	$U_{11} = 0.0116(16)$; $U_{22} = 0.0040(14)$; $U_{33} = 0.0018(15)$; $U_{23} = -0.0008(11)$[b]
Al2 in 4e	(1/4, 0.583 64(13), 0.6621(5))
occ. = 1.00(6)	$U_{11} = 0.0094(14)$; $U_{22} = 0.0087(16)$; $U_{33} = 0.0023(15)$; $U_{23} = 0.0014(12)$[b]
Al3 in 4e	(1/4, 0.700 45(13), 0.1660(5))
occ. = 1.00(6)	$U_{11} = 0.0106(16)$; $U_{22} = 0.0044(14)$; $U_{33} = 0.0032(15)$; $U_{23} = 0.0001(12)$[b]
Al4 in 2b	(1/4, 3/4, 0.5089(7))
occ. = 1.00(8)	$U_{11} = 0.0118(22)$; $U_{22} = 0.0044(21)$; $U_{33} = 0.0029(22)$[c]

[a] Crystal structure data are standardized using the program STRUCTURE TIDY [11].
[b] $U_{12} = U_{13} = 0$; units in nm $\times 10^2$.
[c] $U_{12} = U_{13} = U_{23} = 0$; units in nm $\times 10^2$.

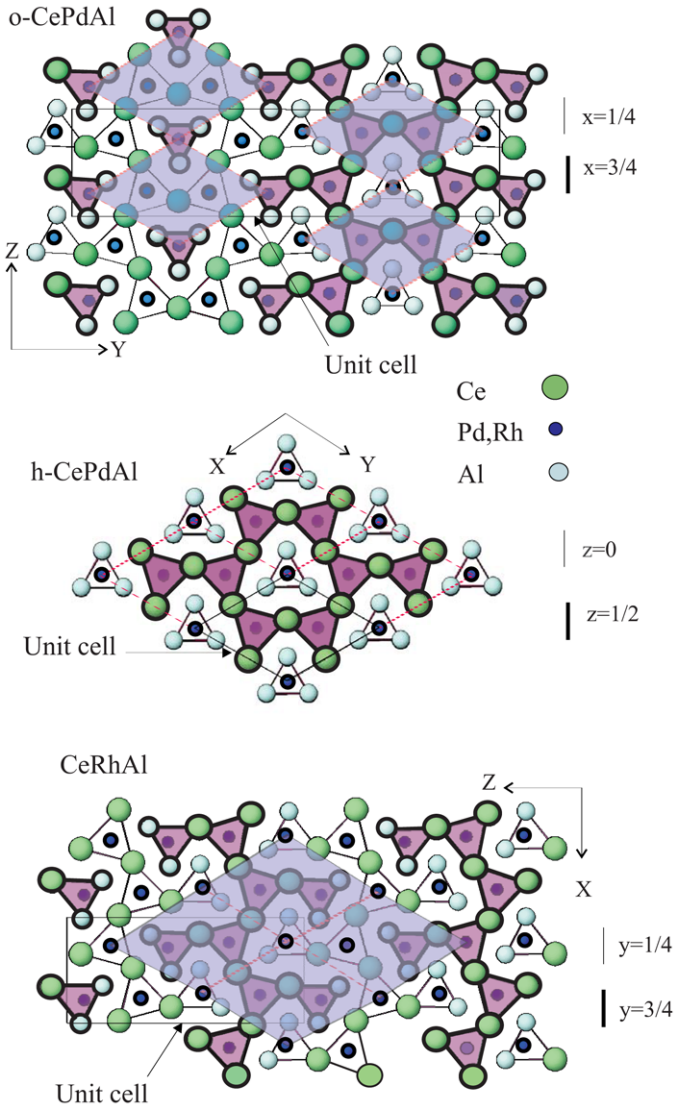

Figure 1. Crystal structure of orthorhombic CePdAl and crystallographic relation to the structures of hexagonal CePdAl and orthorhombic CeRhAl.

strongly distorted cube–octahedra. Considering the connectivity of the coordination figures, the crystal structure of *o*-CePdAl can be presented as a combination of trigonal prisms [Ce_6] and [Ce_2Al_4] centred by the small Pd atoms (figure 1). Six edge-connected [Ce_6] prisms form a ring branched with two [Ce_2Al_4] prisms. Connected via triangular faces, the units are stacked on top of each other in the direction of the a-axis, creating infinite branched tubes. The tubes are edge connected to form walls parallel to the c-axis. In the direction of the b-axis, the walls alternate with similar units shifted by $a/2$ and interleave with their branched parts (figure 1). Each (distorted hexagonal) tube contains an inner column of triangular prisms [Al_6]Pd which are connected via their triangular faces. The inner column and outer tube are shifted by $a/2$, providing tetrakaidecahedral coordination [Ce_3Al_6]Pd for each Pd atom in the inner tube.

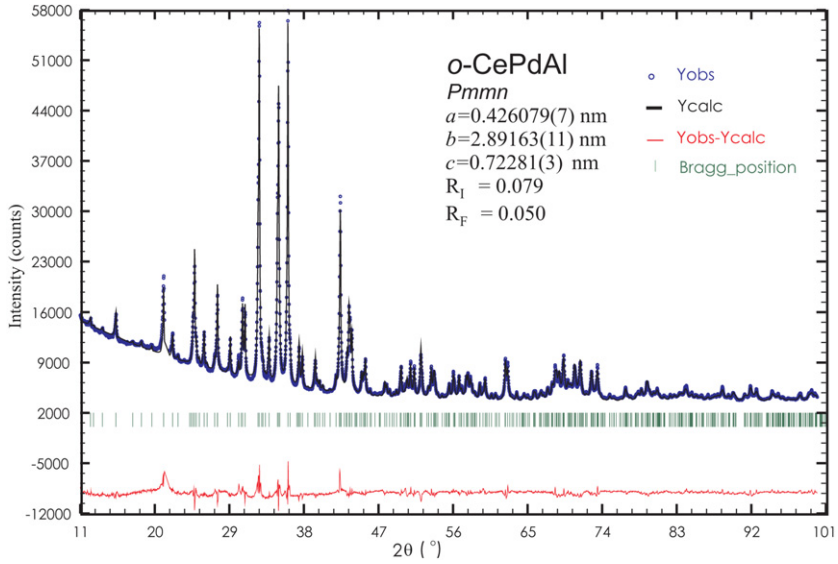

Figure 2. X-ray diffraction pattern of orthorhombic CePdAl.

The centrosymmetric orthorhombic structure of *o*-CePdAl is related to the hexagonal high-temperature modification of CePdAl (*h*-CePdAl) with ZrNiAl type (ordered Fe_2P structure) obtained from as-cast alloys [12]. The hexagonal modification can be used as a base unit in constructing at least two centrosymmetric orthorhombic structures: *o*-CePdAl (this work) and CeRhAl (space group *Pnma*, [13]). Figure 1 illustrates the geometrical relationship between the structures of *h*- and *o*-CePdAl as well as between *h*-CePdAl and CeRhAl. Regions that are related to the unit cell of *h*-CePdAl (ZrNiAl-type) are shaded.

In the present investigation, both modifications of CePdAl were obtained as bulk single-phase materials. Quenching the alloy CePdAl from the melt reveals the *h*-CePdAl structure, while after heat treatment at 900 °C the *o*-CePdAl structure is formed. Thus, one can suppose that *h*-CePdAl and *o*-CePdAl are high- and low-temperature modifications. Figure 2 shows the x-ray powder diffraction pattern of *o*-CePdAl and pattern refinement with the FULLPROF program. No secondary phases were observed. The lattice parameters obtained, $a = 0.426\,079(7)$ nm, $b = 2.891\,63(11)$ nm and $c = 0.722\,81(3)$ nm, are close to the single-crystal data.

In order to characterize the physical behaviour of the novel modification of CePdAl, temperature-dependent magnetic, thermodynamic and transport properties were studied.

Figure 3(a) shows the temperature-dependent magnetic susceptibility χ plotted as χ^{-1} versus T for *o*-CePdAl from 1.8 to 300 K. The almost linear temperature dependence of χ^{-1} above about 50 K refers to the magnetic configuration of the Ce ions, i.e. Ce-$4f^1$. To account for this region quantitatively, a least-squares fit according to the modified Curie–Weiss law, i.e. $\chi = \chi_0 + C/(T - \theta_p)$, was applied. $\chi_0 = 2.6 \times 10^{-4}$ emu mol^{-1} represents a temperature-independent Pauli-like susceptibility, C is the Curie constant yielding an effective moment $\mu_{\rm eff} = 2.35\ \mu_B$, and $\theta_p = -16$ K is the paramagnetic Curie temperature. The effective magnetic moment is close to the theoretical value associated with the Ce^{3+} state, i.e. 2.54 μ_B, indicating a stable $4f^1$ electronic configuration of the Ce ions. The slight curvature of the inverse magnetic susceptibility observed below 50 K is attributed to crystalline electric field (CEF)

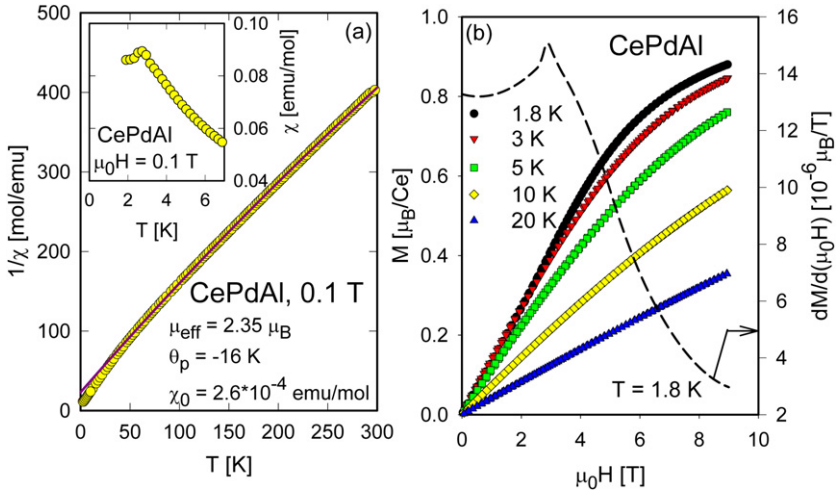

Figure 3. (a) Temperature-dependent magnetic susceptibility χ of *o*-CePdAl plotted as $1/\chi$ versus T. The solid line is a least-squares fit according to the modified CW-law. The inset shows low-temperature details of $\chi(T)$. (b) Isothermal magnetization of *o*-CePdAl taken at various temperatures. The field derivation of the magnetization refers to the right axis.

effects. A substantial density of states near to the Fermi energy is obvious from a relatively large Pauli-like susceptibility and is associated with the 3d band of the Pd sublattice.

The negative paramagnetic Curie temperature refers to antiferromagnetic interactions between the almost localized Ce-4f moments and the conduction electrons. In terms of the Kondo effect, usually present in cerium compounds, the characteristic temperature scale, i.e. the Kondo temperature, can be extracted via $T_K \approx |\theta_p|/4$, suggesting $T_K \approx 4$ K [14].

Below about 2.6 K, a transition into a magnetically ordered state becomes definite from the present susceptibility data (inset, figure 3(a)). In conjunction with isothermal magnetization, antiferromagnetic order can be concluded (compare figure 3(b)). $M(H)$ of o-CePdAl shows no spontaneous order at the lowest temperatures ($T = 1.8$ K) but exhibits a weak metamagnetic phase transition around 3 T. This feature becomes apparent when plotting $\partial M/\partial H$ of o-CePdAl, taken at $T = 1.8$ K (dashed line, figure 3(b), right axis). The ordered moment observed at the lowest temperatures and at our highest applied field is well below 1 μ_B/Ce. Since $M_s = g_j j = 2.14\ \mu_B \gg M_{exptl}$ (Ce: $g_j = 6/7$ and $j = 5/2$), CEF effects can be concluded, responsible for a lifting of the six-fold degenerate ground state of the Ce^{3+} ions into three energetically separated doublets. The Kondo effect also tends to weaken the ordered moment.

Long-range magnetic order is also corroborated from temperature-dependent heat capacity measurements. Results are shown in figure 4. The sharp anomaly at 2.55 K refers to the onset of long-range magnetic order, in excellent agreement with the susceptibility data. The height of the specific heat anomaly, δ, at $T = T_N$ is well below that associated with ordering within an unperturbed crystal field doublet as the ground state ($\delta = 12.5$ J mol^{-1} K^{-1}). In general, such a distinct reduction is attributed to short-range order effects and/or Kondo-type interaction. The latter tends to screen the Ce-4f moments; as a result, both the ordering temperature and the magnetic entropy released at the phase transition are diminished.

Considering the Kondo effect as the primary cause of the observed reduced magnitude of the specific heat anomaly, the resonant-level model of Schotte and Schotte [15] can be used, and long-range magnetic order is incorporated in terms of molecular field theory [16–18].

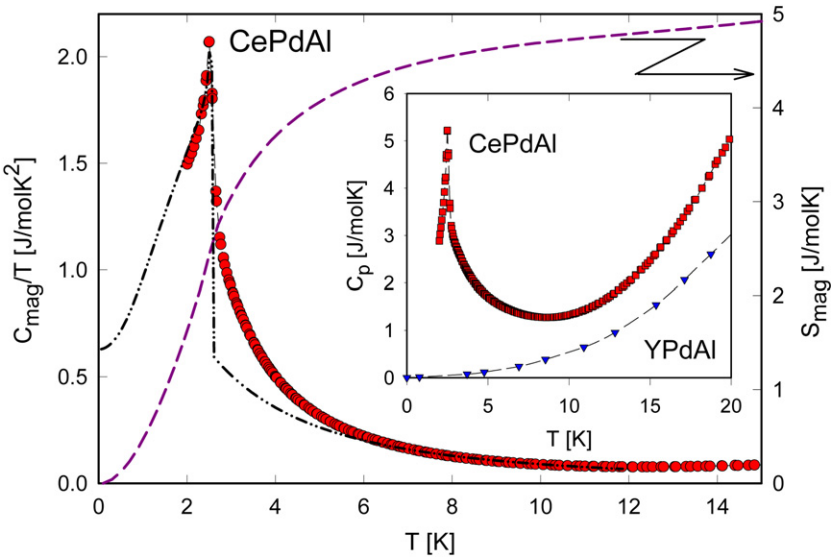

Figure 4. Magnetic contribution to the temperature-dependent specific heat C_{mag} of *o*-CePdAl plotted as C_{mag}/T versus T. The dashed line represents the magnetic entropy S_{mag} and refers to the right axis. The dashed–dotted line is a fit according to equation (4). The inset shows the heat capacity $C_p(T)$ of *o*-CePdAl. $C_p(T)$ of YPdAl is added for comparison.

The temperature-dependent specific heat can be evaluated from the spontaneous magnetization $M(T)$ of an effective $j = 1/2$ system equivalent to a classical two-level system:

$$M(T) = \frac{g\mu_{\mathrm{B}}}{2} \tanh\left(\frac{E}{2k_{\mathrm{B}}T}\right). \tag{1}$$

Here, g is the Landé-factor, μ_{B} is the Bohr magneton and E follows in the mean field theory from

$$E = g\mu_{\mathrm{B}}B_0 = g\mu_{\mathrm{B}}\lambda M = J\frac{M}{M_0}. \tag{2}$$

B_0 refers to the molecular field, λ is the molecular-field constant, J is the s–f coupling constant, and M_0 is the spontaneous magnetization at $T = 0$.

Since the Kondo effect causes a broadening of levels, equation (1) is no longer applicable, demanding the use of the following expression [16]:

$$M(T) = \frac{g\mu_{\mathrm{B}}}{\pi}\mathcal{I}\left[\psi\left(\frac{1}{2} + \frac{\Delta + \mathrm{i}E}{2\pi k_{\mathrm{B}}T}\right)\right]. \tag{3}$$

ψ is the Digamma function. For spin 1/2 systems, $c_{\mathrm{mag}}(T)$ follows then from

$$C_{\mathrm{mag}}(T) = 2k_{\mathrm{B}}\mathcal{R}\left[\frac{z}{T}\left[1 - \left(\frac{z}{T} - \frac{\partial z}{\partial T}\right)\psi'\left(\frac{1}{2} + \frac{z}{T}\right)\right]\right], \tag{4}$$

with $z = (\Delta + \mathrm{i}E(T))/2\pi k_{\mathrm{B}}$. The best agreement between the experimental results and the predictions of equation (4) is revealed when taking $J = 11$ K and $T_{\mathrm{K}} = 4.8$ K (dashed–dotted line, figure 4). Assuming that the Kondo effect is absent in o-CePdAl, i.e. $T_{\mathrm{K}} = 0$, the deduced s–f coupling constant $J = 11$ K would lead to magnetic ordering around $T_{\mathrm{N}}^0 = 5.5$ K, equivalent to $T_{\mathrm{N}} = J/2$. Of course, this phenomenological model is unable to account for short-range ordering effects above the transition temperature, responsible for the

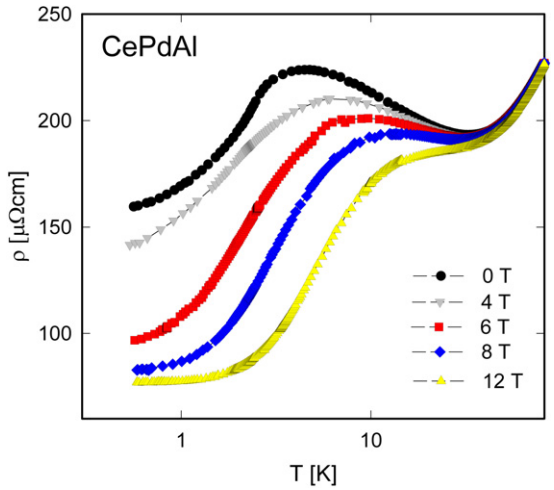

Figure 5. Temperature-dependent resistivity ρ of *o*-CePdAl for various values of externally applied magnetic fields.

observed broadening of the magnetic phase transition (compare the differences in figure 4 of the experimental data and the fit between 3 and 5 K). The discrepancy between the calculated ordering temperature and the observed one sheds light on further implications of the Kondo effect, which also reduces the magnitude of the spontaneous moments. Taking both $J = 11$ K and $T_K = 4.8$ K (equation (3)) would result in downsizing of the ordered moments to about 60%, when compared to an otherwise unperturbed CEF ground state.

The Sommerfeld value γ follows from the above model as 620 mJ mol^{-1} K^{-2}, which is larger than the one observed for hexagonal CePdAl. Here, it should be noted that the simultaneous presence of RKKY interaction and the Kondo effect reverses the well-known relation $T_K \propto 1/\gamma$ in this model. Rather, keeping the RKKY interaction constant while increasing the Kondo interaction strength causes γ to rise within a limited range of the ratio J/T_K. If, for example, T_K increases to 6.5 K, a hypothetical Sommerfeld value of 1070 mJ mol^{-1} K^{-2} would result, retaining $J = 11$ K.

Anomalous features, associated with the Kondo effect, are also derived from the entropy data (solid line, figure 4), which amount to 3 J mol^{-1} K^{-1} at $T = T_N$, while $R \ln 2$ is not recovered below 22 K. Both quantities indicate that magnetic ordering occurs in a CEF doublet as the ground state [19]; the first excited level of this compound, however, is well separated from this ground state.

Distinct hints to the Kondo effect present in this orthorhombic modification of CePdAl stem from the temperature-dependent resistivity $\rho(T)$. Measurements performed down to 400 mK and fields up to 12 T are shown in figure 5. The most important characteristics found at zero external field are a negative slope of $\rho(T)$ below about 20 K, and a maximum at 4.5 K. While the former refers to the Kondo effect in the CEF ground state, the latter can be considered as a signature of coherence, originated from the periodic arrangement of the Ce ions in o-CePdAl. The rapid decrease of the resistivity below that maximum results from the onset of long-range magnetic order in the vicinity of 2.5 K, in good agreement with both susceptibility and specific heat results. The application of external fields causes an overall decrease in the electrical resistivity as well as a shift of the low-temperature resistivity maximum to higher temperatures. These observations are typical features of Kondo lattices where the quenching of

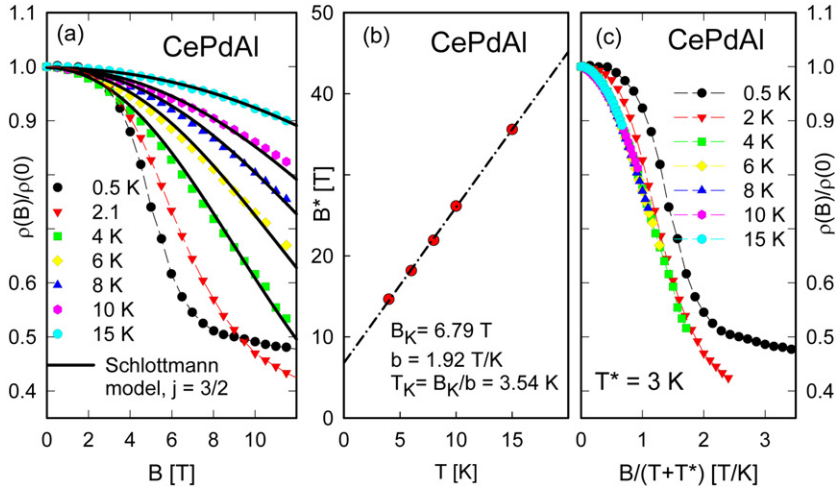

Figure 6. (a) Isothermal magnetoresistance $\rho(B)/\rho(0)$ versus B of o-CePdAl for various temperatures. The solid line is a least-squares fit according to the Schlottmann model. (b) Temperature-dependent Kondo field B^* of o-CePdAl. (c) Isothermal magnetoresistance $\rho(B)/\rho(0)$ versus $B/(T + T^*)$ of o-CePdAl. The scaling temperature $T^* = 3$ K.

the Kondo interaction by the external magnetic field depletes the scattering intensity and thus reduces $\rho(T)$.

Isothermal magnetoresistance measurements are shown in figure 6(a) as $\rho(B)/\rho(0)$ versus B, where $\rho(B)$ and $\rho(0)$ are the resistivity data taken at external and zero fields, respectively. $\rho(B)/\rho(0)$ of o-CePdAl shows two distinct regimes: (i) isothermal curves below the phase transition temperature exhibit distinct changes of the slope, as a consequence of field-driven spin reorientations; (ii) the field dependence of $\rho(B)/\rho(0)$ in the paramagnetic temperature range of o-CePdAl resembles typical Kondo lattices and thus can be described in terms of the model of Schlottmann [20]. Results of least-squares fits are shown as solid lines, revealing temperature-dependent characteristic Kondo fields. Plotting these fields as a function of temperature enables to derive the Kondo field B^* at zero temperature; thus the Kondo temperature can be determined independently [21]. An extrapolation to zero yields $B^* = 6.79$ T (figure 6(b)). Together with the slope $b = 1.92$ T K^{-1}, T_K follows as $T_K \approx 3.5$ K. The model of Schlottmann indicates that a single characteristic energy scale, i.e. the Kondo temperature T_K, is the relevant scale of the system, which determines both the shape and the magnitude of $\rho(B)/\rho(0)$. In order to demonstrate these scaling features present in o-CePdAl, $\rho(B)/\rho(0)$ is plotted versus $B/(T + T^*)$ (see figure 6(c)). T^* is chosen such that all the data taken at temperatures $T > T_N$ match a single curve. The characteristic temperature ($T^* = 3$ K) thus deduced agrees well with that obtained from the heat capacity measurement and also with the above analysis in terms of the model of Schlottmann [20].

4. Summary

Crystal structure, transport, magnetic and thermodynamic properties were studied for the new orthorhombic low-temperature modification of equiatomic CePdAl. Some of the bulk properties of orthorhombic CePdAl resemble closely CePdAl with a hexagonal ZrNiAl type of structure. While, however, the former shows long-range magnetic order around 2.55 K, the latter exhibits the magnetic instability at slightly larger temperatures ($T_N = 2.7$ K, [3]), but the

shapes and distinct features of the various physical quantities with respect to their temperature and field dependences appear to be almost unchanged. This observation points to the dominant role of interatomic distances and/or binding lengths, which predefines macroscopic physical properties; slight differences in the crystal structure then cause in many cases only limited corrections. The fact that the effective magnetic moment of orthorhombic CePdAl is near to that associated with the Ce^{3+} state evidences that all the Ce ions, occupying four different crystallographic lattice sites, possess the $4f^1$ electronic configuration. An enhanced Sommerfeld value γ of orthorhombic CePdAl, and thus an increased value of T_K in the context of similar transition temperatures, may overcompensate the effect of the absent geometrical frustration to reduce the temperature of the magnetic instability.

Acknowledgments

Work supported by Austrian FWF P 18054 and the Austrian–Russian Technical Scientific Exchange Program (P I.18/04) via the Russian Foundation for Basic Research, RFBR Grant No. 05-03-33045.

References

[1] Dwight A E 1984 *J. Less-Common Met.* **102** L9
[2] Hulliger F 1995 *J. Alloys Compounds* **218** 44
[3] Kitazawa H, Matsushita A, Matsumoto T and Suzuki T 1994 *Physica* B **199/200** 28
[4] Dönni A, Ehlers G, Maletta H, Fischer P, Kitazawa H and Zolliker M 1996 *J. Phys.: Condens. Matter* **8** 11213
[5] Nishiyama M, Oyamada A, Maegawa S, Goto T and Kitazawa H 2003 *J. Phys.: Condens. Matter* **15** S2267
[6] Akamura S, Isikawa Y, Kuwai T, Mizushima T, Sakurai J and Uwatoku Y 2002 *Physica* B **312/313** 466
[7] Sheldrick G M 1997 *Program SHELXS97 and SHELXL97* University of Göttingen, Germany
[8] Rodriguez-Carvajal J 1990 *Abstracts of the Satellite Meeting on Powder Diffraction of the XV Cong. of the IUCr (Toulouse, France)* p 127
[9] Roisnel T and Rodriguez-Carvajal J 2001 *Materials Science Forum, EPDIC7: Proc. European Powder Diffraction Conf.* vol 378–381, p 118
[10] Bauer E, Berger St, Paul Ch, Della Mea M, Hilscher G, Michor H, Reissner M, Steiner W, Grytsiv A, Rogl P and Scheidt E-W 2002 *Phys. Rev.* B **66** 214421
[11] Gelato L M and Parthé E 1987 *J. Appl. Crystallogr.* **20** 139
[12] Xue B, Schwer H and Hulliger F 1994 *Acta Crystallogr.* C **50** 338
[13] Schwer H and Hulliger F 1997 *J. Alloys Compounds* **259** 249
[14] Hewson A C 1993 The Kondo problem to heavy fermions *Cambridge Studies in Magnetism* vol 2 (Cambridge: Cambridge University Press)
[15] Schotte K D and Schotte U 1975 *Phys. Lett.* A **55** 38
[16] Bredl C D, Steglich F and Schotte K D 1978 *Z. Phys.* B **29** 327
[17] Braghta A 1989 *PhD Thesis* University of Strasbourgh
[18] Besnus M J, Braghta A, Hamdaoui N and Meyer A 1992 *J. Magn. Magn. Mater.* **104–107** 1385
[19] Desgranges H U and Schotte K D 1982 *Phys. Lett.* A **91** 240
[20] Schlottmann P 1983 *Z. Phys.* B **51** 223
[21] Batlogg B, Bishop D J, Bucher E, Golding B, Ramirez A P, Fisk Z, Smith J L and Ott H R 1987 *J. Magn. Magn. Mater.* **64–67** 441